Volume 60
Number 82
21 October 2024
Pages 11599–11800

ChemComm

Chemical Communications

rsc.li/chemcomm

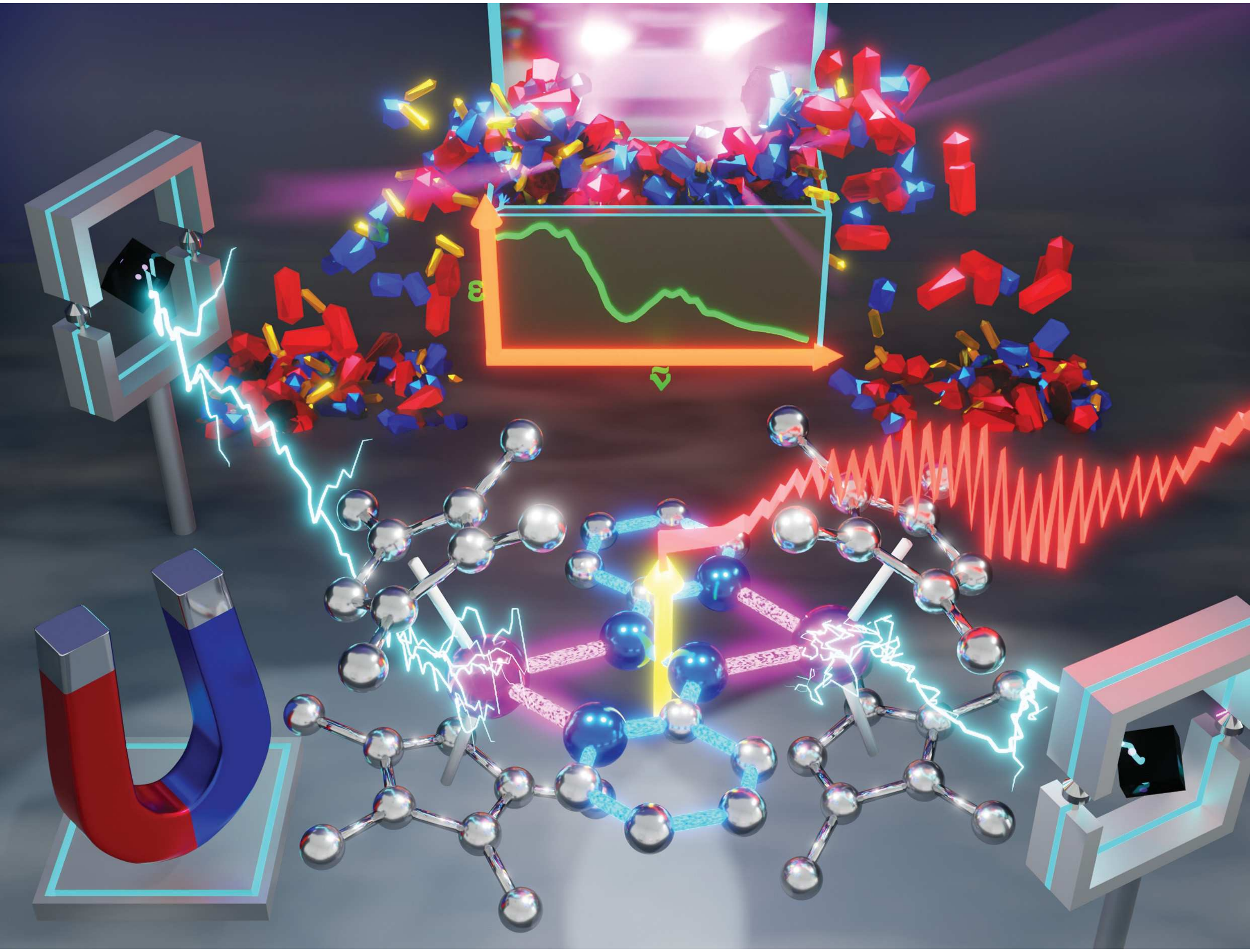

ISSN 1359-7345

ROYAL SOCIETY
OF **CHEMISTRY**

COMMUNICATION
Francis Delano and Selvan Demir
Implementation of 2,2′-azobispyridine radical mono- and dianions in dinuclear rare earth metal complexes

60 YEARS
ANNIVERSARY

ChemComm

COMMUNICATION

View Article Online
View Journal | View Issue

Cite this: *Chem. Commun.*, 2024, **60**, 11702

Received 30th June 2024,
Accepted 16th August 2024

DOI: 10.1039/d4cc03222e

rsc.li/chemcomm

Implementation of 2,2′-azobispyridine radical mono- and dianions in dinuclear rare earth metal complexes†

Francis Delano IV and Selvan Demir *

The seminal isolation of a dinuclear rare earth metal complex comprising a bridging 2,2′-azobispyridyl radical anion, [(Cp^{tet}$_2$Y)$_2$(μ-abpy$^•$)](BPh$_4$), is presented, which was obtained from a one-electron chemical oxidation of [(Cp^{tet}$_2$Y)$_2$(μ-abpy)]. The unprecedented compounds were characterized by crystallography, spectroscopy and DFT computations. The radical character was proven by EPR spectroscopy.

The inclusion of hetero redox-active ligands capable of housing several electrons in the primary coordination sphere of metal ions is a key design principle for applications in metal–ligand cooperativity and quantum information science.[1,2] Notably, the inclusion of radical-bridging ligands, including $N_2^{3-•}$,[3,4] can lead to strong magnetic exchange coupling when paired with highly magnetically anisotropic lanthanide ions, resulting in remarkable radical-bridged single-molecule magnets. Azoaromatic ligands are exceptionally attractive owing to their low-lying π* molecular orbital capable of electron uptake and their ability to undergo *cis-*/*trans*-photoisomerization which has found use in applications of chemosensors,[5,6] information storage,[7] and smart surface materials.[8] The electron transfer flexibility innate to the azoaromatic class of ligands has also provided insight into biologically relevant processes such as the reduction of N_2.[9]

Since its first application in coordination chemistry in 1969,[10] 2,2′-azobispyridine (abpy) has garnered much interest. The multiple coordination sites coupled with the stable *cis*- and *trans*-isomers enables several accessible coordination modes.[11] Recently, we reported the first rare earth complex containing an azopyridyl radical anion, a rare tridentate coordination geometry of abpy, where binding to the metal centre occurs through both pyridyl rings and one nitrogen of the azo unit.[12] Since then, further conformations of abpy have been revealed such as a seven-membered chelation mode.[13]

The reaction of Cp^{tet}$_2$Y(BPh$_4$) with abpy in toluene at 90 °C followed by the addition of two equiv. of potassium graphite afforded [(Cp^{tet}$_2$Y)$_2$(μ-abpy)] (Cp^{tet} = 1,2,3,4-tetramethylcyclopentadienyl), **1**, eqn (1). The elevated temperature is necessary for the formation of **1** and is attributed to the *cis-*/*trans*-isomerisation energy barrier of the azo-functionality (ΔE_{iso} = 25.2 ± 0.6 kJ mol^{-1}).[14] Notably, the mononuclear complex Cp^{tet}$_2$Y(abpy$^•$) is synthesized in THF at room temperature.[12]

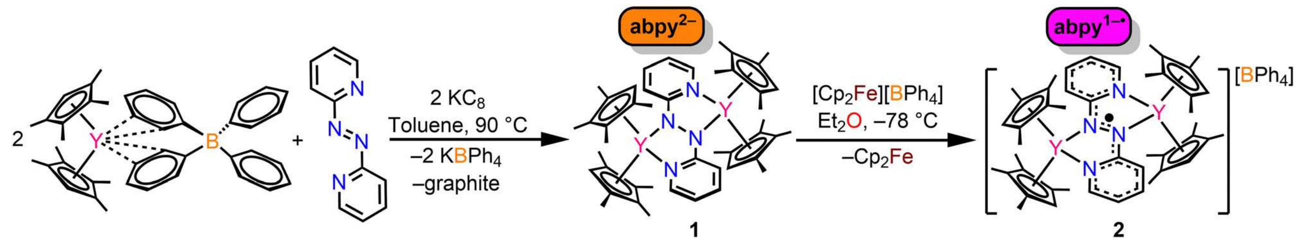

(1)

Red, block-shaped crystals of **1**, suitable for single-crystal X-ray diffraction analysis were grown from concentrated toluene solution at −35 °C in 20% yield, Fig. S1 (ESI†). **1** constitutes the first crystallographically characterized dinuclear rare earth metal complex containing a 2,2′-azobispyridine ligand.

Department of Chemistry, Michigan State University, 578 South Shaw Lane, East Lansing, Michigan, 48824, USA. E-mail: sdemir@chemistry.msu.edu

† Electronic supplementary information (ESI) available. CCDC 2366736 and 2366737. For ESI and crystallographic data in CIF or other electronic format see DOI: **https://doi.org/10.1039/d4cc03222e**

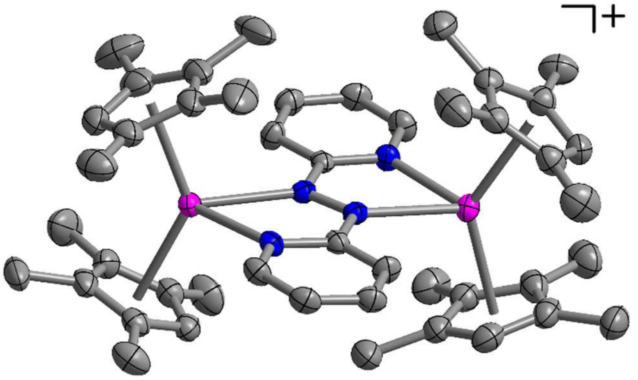

Fig. 1 Structure of the cation of [(Cp$^{tet}{}_2$Y)$_2$(μ-abpy$^{\bullet}$)][BPh$_4$], **2**, in a crystal of [(Cp$^{tet}{}_2$Y)$_2$(μ-abpy$^{\bullet}$)][BPh$_4$]·CH$_2$Cl$_2$·1.5C$_7$H$_8$, with thermal ellipsoids drawn at 50%. Pink, blue, and grey ellipsoids represent Y, N, and C atoms, respectively. The BPh$_4{}^-$ counterion, hydrogen atoms, and co-crystallized solvent molecules have been omitted for clarity. Selected interatomic distances (Å) and angles (°): Y–N$_{py}$ = 2.378(4), 2.389(4); Y–N$_{azo}$ = 2.425(4), 2.428(3); Y1–Cnt = 2.339 and 2.369 Y2–Cnt = 2.359, 2.343; Cnt–Y1–Cnt = 134.1; Cnt–Y2–Cnt = 132.7; N–N = 1.352(4).

1 crystallises in the monoclinic space group $P2_1/n$, where the asymmetric unit contains half of the abpy^{2-} ligand and one [Cp$^{tet}{}_2$Y]$^+$ metallocene moiety. The abpy ligand adopts an ''S-frame'' binding motif,[15] where each metal centre is bridged by the abpy through ligation to one pyridyl and one azo nitrogen fostering two five-membered chelate rings.

Each Y^{III} centre is eight-coordinate ligated by two η^5–(Cp^{tet})$^-$ ligands and one pyridyl– and azo– nitrogen from the abpy ligand. The N–N bond distance of 1.404(4) Å is in excellent agreement with the single bond of hydrazine (1.416(4) Å),[16] indicative of a bridging, dianionic ligand. The Y–N$_{py}$ distance (2.396(3) Å) is slightly longer than the respective Y–N$_{azo}$ distance of 2.362(3) Å and is attributed to the increased anionic charge on the azo-group relative to the pyridyl nitrogen atoms.

In complexes, the redox-active abpy ligand can exist as neutral, radical, and dianionic forms, respectively, where consecutive addition of electrons to the π* lowest unoccupied molecular orbital corresponds to an elongation of the central N–N bond.[11] To probe the accessibility of the radical oxidation state for abpy, **1** was oxidised by one electron through the use of the oxidising agent [Cp$_2$Fe][BPh$_4$] at −78 °C to yield the abpy radical-bridged diyttrium complex [(Cp$^{tet}{}_2$Y)$_2$(μ-abpy$^{\bullet}$)](BPh$_4$) (**2**). Black crystals of **2**, suitable for single-crystal X-ray diffraction analysis, were grown from slow evaporation of a 1:1 dichloromethane : toluene solution at −35 °C in 41% yield, Fig. 1. **2** constitutes the first dinuclear rare earth complex bearing an abpy radical ligand. Following oxidation, evidently the abpy ligand maintains its ''S-frame'' binding motif which results in two five-membered chelate rings sharing the azo-functionality. The N$_{azo}$–N$_{azo}$ distance of 1.352(4) Å is shorter than the corresponding distance in **1** and longer than the N═N double bond of free abpy (1.245(1) Å).[17] This hints at a bond order of 1.5 and indeed, the found N$_{azo}$–N$_{azo}$ distance in **2** is in accordance with the distance observed for a abpy radical anion.[11] The Y–N$_{azo}$ interatomic distance of 2.425(4) Å in **2** is slightly elongated relative to **1** (Δ = 0.063 Å) presumably originating from the reduced anionic charge on the bridging ligand. In addition, the intermetallic Y···Y distances are 5.554(1) Å and 5.662(2) Å for **1** and **2**, respectively. This lengthening by 0.11 Å is similarly attributed to charge on the bridging ligand.

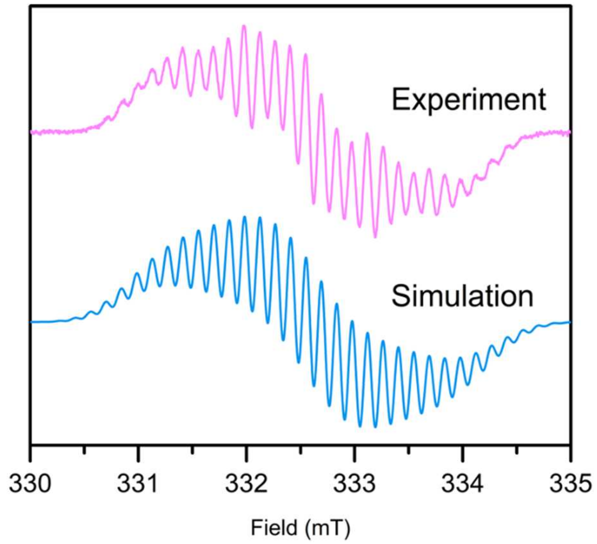

Fig. 2 X-band cw-EPR spectra of [(Cp$^{tet}{}_2$Y)$_2$(μ-abpy$^{\bullet}$)][BPh$_4$], **2**, in dichloromethane solution at 298 K. The pink line represents experimental data, whereas the blue line constitutes the simulated EPR spectrum. Simulation data: spin system of two ^{14}N, two ^{14}N, four ^{1}H, four ^{1}H, four ^{1}H, and two ^{89}Y nuclei, A(^{14}N) = 4.82 MHz, A(^{14}N) = 15.79 MHz, A(^{1}H) = 7.50 MHz, A(^{1}H) = 3.49 MHz, A(^{1}H) = 1.05 MHz, A(^{89}Y) = 4.08 MHz, g = 2.0028; lwpp = 0.072.

To further probe the electronic structure of **2**, the X-band EPR spectrum was collected and simulated at 298 K, Fig. 2. The intensity normalized cw-EPR spectrum of **2** consists of 27 main lines centred at 332.6 mT, corresponding to a g-value of 2.0028, very close to that of a free electron (g = 2.0023).[18] The spectrum of **2** was simulated with hyperfine couplings arising from the N and H nuclei of the abpy ligand, the Y metal centre and H atoms of the Cp^{tet} ancillary ligand scaffold. The relevant hyperfine coupling constants are provided in the caption of Fig. 2.

Similar hyperfine couplings were employed to simulate the cw-EPR spectrum of the mononuclear complex Cp$^{tet}{}_2$Y(abpy$^{\bullet}$).[12] However, the symmetric ''S-frame'' binding motif in **2** facilitates the simulation of the spectrum. The experimentally determined hyperfine couplings for the nitrogen atoms of 15.79 MHz and 4.82 MHz are comparable to the mononuclear analogue (15.2, 11.4 and 4.4 MHz), and suggest that the majority of the electronic spin resides on the azo moiety, consistent with the present structural distortions. Typical of a π-radical, an odd-alternate distribution of spin density occurs on the pyridyl functional group, resulting in two groupings of the eight ligand protons (7.50 and 3.49 MHz). A small contribution (1.05 MHz) stemming from the ring protons of the Cp^{tet-} rings was required for a satisfactory simulation of the spectrum. The 4.08 MHz coupling attributed to ^{89}Y ($S = \frac{1}{2}$) is similar to those obtained for dinuclear compounds innate to open-shell bridging ligands,[19,20] but is substantially smaller than the expected value for an organometallic Y^{II} complex.[21,22] Notably, the magnitude of

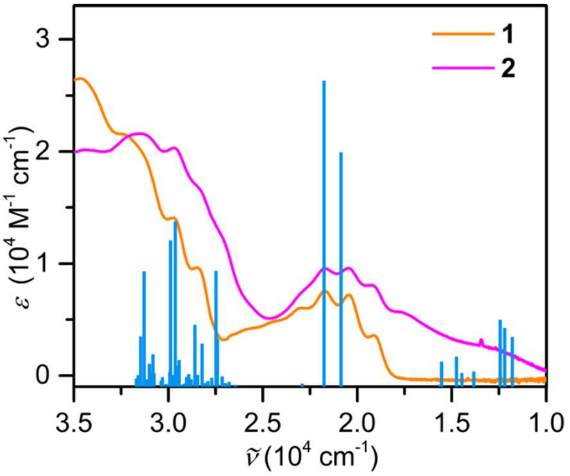

Fig. 3 UV-vis absorption spectra of $[Cp^{tet}{}_2Y]_2(\mu\text{-abpy})$, **1**, and $[(Cp^{tet}{}_2Y)_2(\mu\text{-abpy}^{\bullet})][BPh_4]$, **2**, in dichloromethane solution. The orange and pink lines represent experimental data for **1** and **2**, respectively, whereas the light blue lines constitute the calculated TDDFT transitions for **2**.

the ^{89}Y hyperfine contribution has a minimal effect on the line shape of the simulated spectra, likely owing to the small gyromagnetic ratio of the nucleus (-1.31×10^7 rad s^{-1} T^{-1}).[23] To determine a suitable ^{89}Y hyperfine interaction, DFT calculations were employed to estimate both the *g*–tensor and A-tensor of the metal centre and bridging ligand. The methods for the calculation and the computationally-derived hyperfine coupling constants are provided in the ESI.† The magnitudes of the computationally-derived hyperfine coupling constants match well with those obtained experimentally and are provided in Table S5 (ESI†).

The electronic absorption spectrum of both **1** and **2** were recorded from 220 to 1000 nm in dichloromethane solutions which exhibit several transitions in the visible region of the spectrum, Fig. 3. In both cases, each main band exhibits four shoulders which potentially originates from overlapping transitions stemming from the preferred orientation of the cyclopentadienyl ligands, where this interpretation is supported by four distinct resonances in the ^{1}H NMR spectrum of **1**, Fig. S5 (ESI†). The steric bulk induced by the methyl substituents of the cyclopentadienyl ligands together with the close intermetallic distances (5.554(1) Å (**1**) and 5.662(2) Å (**2**)) may prohibit the rotation of the cyclopentadienyl rings, resulting in a preferred orientation.

The very low-lying abpy-centred π^* molecular orbital gives rise to several π–π^* transitions, typically residing between 384 and 544 nm.[24] To gain insight into the photophysical properties of **1** and **2**, time-dependent density functional theory (TDDFT) calculations were performed on the optimised geometries of **1** and **2**. The calculated transitions are plotted alongside the experimental absorption spectra in Fig. 3, S13–S15 (ESI†), and the tabulated data are provided in Tables S3 and S4 (ESI†). As expected, several metallocene to abpy-based transitions occur between 312 nm (3.21×10^4 cm^{-1}) and 354 nm (2.82×10^4 cm^{-1}) for both **1** and **2**. Similar to the free ligand, multiple π–π^* transitions ascribed to the abpy unit appear in the visible region of the spectrum (497 nm, 2.01×10^4 cm^{-1} for **1**; 496 nm, 2.02×10^4 cm^{-1} for **2**). The formation of the radical monoanion is concurrent with the emergence of a low energy absorption band, typical of a π–based radical.[25]

The electron transfer processes of **1** were probed *via* cyclic voltammetry, Fig. S16 (ESI†), where the measurements were conducted in dichloromethane using 250 mM $[N^nBu_4][PF_6]$ as a supporting electrolyte. The cyclic voltammogram reveals two independent redox processes positioned at −489 and 660 mV *vs.* Fc^+/Fc, respectively. Both of these electrochemical events are ascribed to the redox-active bridging abpy ligand. Stabilization of the RE metals in oxidation states outside of the archetypal +III are typically highly reactive and electrochemical processes ascribed to the $RE^{II/III}$ redox couples are generally located at significantly more reducing potentials.[22,26] This interpretation is in accordance with the computationally determined abpy-localized lowest unoccupied molecular orbital. The electrochemically reversible feature located in the reductive (−489 mV) region of the voltammogram is attributed to the $abpy^{2-/1-\bullet}$ redox couple and is congruent with the observed chemical reactivity of **1** towards the oxidising agent $[Cp_2Fe][BPh_4]$. By contrast, the application of more oxidative potentials gives rise to an irreversible redox feature at 660 mV, assigned to the $abpy^{1-/0}$ redox couple. The irreversible nature of this event points at the onset of a chemical process (*i.e.* degradation of the bimetallic species), possibly due to the decreased Lewis basicity of the chelating nitrogen atoms as a result of the reduced anionic charge. Cyclic voltammograms of **2** were not measured owing to degradation of the complex in the electrolyte solution.

Notably, electrochemical studies on organometallic transition metal abpy complexes are scarce, where the only known Cp-based system constitutes the mononuclear complex, $Cp^{tet}{}_2Y(abpy^{\bullet})$.[12] Intriguingly, the redox processes examined in the mononuclear system take place at significantly more negative potentials, potentially caused by the additional electropositive metal in **1** relative to the mononuclear complex.

The electronic structure of both **1** and **2** were investigated through DFT. The experimental methods of all calculations are provided in the ESI.† A comparison of the crystallographically determined geometry with those predicted computationally reveal that the unrestricted TPSSh functional best represents the physical structure, Table S2 (ESI†). Hence, a final geometry optimisation was completed employing this functional including a def2-TZVP description on Y and N. To allow for comparison of the predicted electronic structure, the geometry of **1** was also optimised using the same method.

The frontier orbitals of **1** and **2** are shown in Fig. S18 and S20 (ESI†), respectively. In both cases the HOMO is centred on the bridging abpy ligand, consistent with the observed electrochemical behaviour. Expectedly, the singly occupied molecular orbital (SOMO) is largely localized on the bridging unit and features small contributions from the ancillary Cp^{tet} ligands. Consequently, the total spin density, Fig. 4, is mainly localized on the bridging ligand with small contributions from both the metal centres and Cp ligands, which description is in agreement with the simulated hyperfine coupling parameters, Fig. 2.

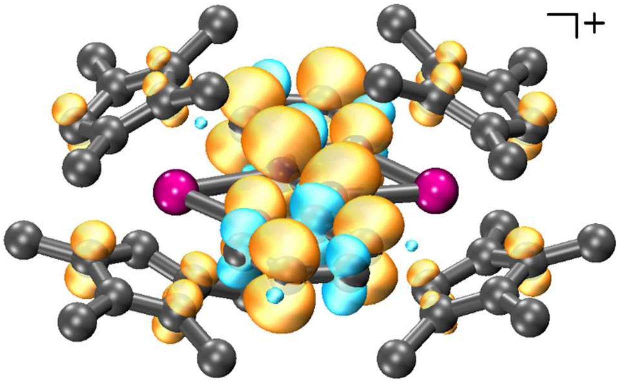

Fig. 4 Calculated spin density map of $[(Cp^{tet}{}_2Y)_2(\mu\text{-abpy}^{\bullet})][BPh_4]$, **2** (isovalue: 0.04). Pink, blue, and grey spheres represent Y, N, and C atoms, respectively. H atoms have been omitted for clarity.

The bonding picture of both **1** and **2** were explored through a natural localized molecular orbital (NLMO)[27] analysis. The NLMO analysis suggests an ionic bonding situation between the ligands and Y^{III} ions, as all metal–ligand interactions are located within the second-order perturbation analysis. The strongest interactions arise from donations of the lone pairs of the azo nitrogen atoms to the metal centre (summed contributions of 20.81 kcal mol^{-1} and 27.98 kcal mol^{-1} for **1** and **2**, respectively). The donations from the pyridyl nitrogen atoms are substantially weaker, affording summed contributions of 7.66 kcal mol^{-1} and 12.2 kcal mol^{-1} which are attributed to the increased charge on the azo nitrogen atoms relative to the pyridyl nitrogen atoms.

In conclusion, the first radical-bridged rare earth metal complex containing a bridging 2,2-azobispyridine (abpy) ligand, $[(Cp^{tet}{}_2Y)_2(\mu\text{-abpy}^{\bullet})](BPh_4)$, **2**, is presented. **2** was synthesized through a one-electron chemical oxidation of the neutral complex $[(Cp^{tet}{}_2Y)_2(\mu\text{-abpy})]$, **1**. Notably, both **1** and **2** constitute the first dinuclear rare earth metal complexes with a bridging abpy ligand. The radical nature of the abpy ligand was proven by X-ray crystallography, EPR Spectroscopy, and DFT computations. The bridging abpy ligand adopts a "S-frame" bonding motif forming two five membered chelate rings containing two $[Cp^{tet}{}_2Y]^+$ units. Simulation of the experimental EPR spectrum suggest that the spin largely resides on the bridging abpy ligand and is primarily located on the azo functionality. The diverse coordination modes, range of attainable oxidation states, and potential for functionalizing the abpy ligand, offer a unique platform in the realm of rare earth metal chemistry. The development of suitable synthetic routes to higher nuclearity rare earth metal compounds comprising abpy bridging ligands may provide a unique access to technologically relevant compounds including photo-isomeric and spin-based materials. Exploiting the synergy of azopyridine ligands with optically emissive lanthanides such as Tb^{III} and Eu^{III} may represent yet another exciting frontier of research.

S. D. thanks the National Science Foundation (NSF) for grant No. CHE-2339595 (CAREER), the Department of Chemistry at MSU for start-up funds, and the Institute for Cyber-Enabled Research for support. Funding for a single-crystal X-ray diffractometer was provided by NSF under grant No. CHE-1919565. We thank Ernesto Castellanos and Saroshan Deshapriya for experimental assistance.

Data availability

CCDC 2366736 and 2366737 contains the supplementary crystallographic data for this paper. The other characterization data supporting this article have been included as part of the ESI.†

Conflicts of interest

There are no conflicts to declare.

Notes and references

1 J. McGuire, H. N. Miras, J. P. Donahue, E. Richards and S. Sproules, *Chem. – Eur. J.*, 2018, **24**, 17598–17605.
2 M. E. Czaikowski, S. W. Anferov and J. S. Anderson, *Chem. Catal.*, 2024, **4**, 100922.
3 S. Demir, M. I. Gonzalez, L. E. Darago, W. J. Evans and J. R. Long, *Nat. Commun.*, 2017, **8**, 2144.
4 J. D. Rinehart, M. Fang, W. J. Evans and J. R. Long, *Nat. Chem.*, 2011, **3**, 538–542.
5 J. Isaad and A. Perwuelz, *Tetrahedron Lett.*, 2010, **51**, 5810–5814.
6 A. Abdollahi, H. Roghani-Mamaqani and B. Razavi, *Prog. Polym. Sci.*, 2019, **98**, 101149.
7 Z. F. Liu, K. Hashimoto and A. Fujishima, *Nature*, 1990, **347**, 658–660.
8 H. S. Lim, J. T. Han, D. Kwak, M. Jin and K. Cho, *J. Am. Chem. Soc.*, 2006, **128**, 14458–14459.
9 M. J. Chalkley, M. W. Drover and J. C. Peters, *Chem. Rev.*, 2020, **120**, 5582–5636.
10 D. A. Baldwin, A. B. P. Lever and R. V. Parish, *Inorg. Chem.*, 1969, **8**, 107–115.
11 S. Panda, S. Dhara, A. Singh, S. Dey and G. Kumar Lahiri, *Coord. Chem. Rev.*, 2023, **475**, 214895.
12 F. Delano IV, E. Castellanos, J. McCracken and S. Demir, *Chem. Sci.*, 2021, **12**, 15219–15228.
13 J. Long, L. Rocard, E. Van Elslande, P. Retailleau, J. Xie and N. Bogliotti, *Chem. – Eur. J.*, 2023, **29**, e202301301.
14 M. Zhu and L. Yu, *J. Therm. Anal. Calorim.*, 2018, **132**, 463–469.
15 W. Kaim, *Coord. Chem. Rev.*, 2001, **219–221**, 463–488.
16 S. Patai, *Chemistry of the Hydrazo, Azo, and Azoxy groups*, Wiley, 1975.
17 H. Bock, R. Dienelt, H. Schödel and T. T. H. Van, *Struct. Chem.*, 1998, **9**, 279–288.
18 M. M. Roessler and E. Salvadori, *Chem. Soc. Rev.*, 2018, **47**, 2534–2553.
19 F. Benner and S. Demir, *Chem. Sci.*, 2022, **13**, 5818–5829.
20 F. Delano IV, S. Deshapriya and S. Demir, *Inorg. Chem.*, 2024, **63**, 9659–9669.
21 J. F. Corbey, D. H. Woen, C. T. Palumbo, M. E. Fieser, J. W. Ziller, F. Furche and W. J. Evans, *Organometallics*, 2015, **34**, 3909–3921.
22 R. Jena, F. Benner, F. Delano IV, D. Holmes, J. McCracken, S. Demir and A. L. Odom, *Chem. Sci.*, 2023, **14**, 4257–4264.
23 A. Venkatesh, M. J. Ryan, A. Biswas, K. C. Boteju, A. D. Sadow and A. J. Rossini, *J. Phys. Chem. A*, 2018, **122**, 5635–5643.
24 M. Krejcik, S. Zalis, J. Klima, D. Sykora, W. Matheis, A. Klein and W. Kaim, *Inorg. Chem.*, 1993, **32**, 3362–3368.
25 M. Schultz, J. M. Boncella, D. J. Berg, T. D. Tilley and R. A. Andersen, *Organometallics*, 2002, **21**, 460–472.
26 M. R. MacDonald, J. E. Bates, J. W. Ziller, F. Furche and W. J. Evans, *J. Am. Chem. Soc.*, 2013, **135**, 9857–9868.
27 A. E. Reed and F. Weinhold, *J. Chem. Phys.*, 1985, **83**, 1736–1740.